arXiv:1411.2256v1 [physics.ao-ph] 9 Nov 2014

Data-Driven Prediction of Thresholded Time Series of Rainfall and SOC models

Anna Deluca,[1,*] Nicholas R. Moloney,[2] and Álvaro Corral[3,4,†]

[1] *Max-Planck-Institut für Physik Komplexer Systeme, Nöthnitzer Strasse 38, D-01187 Dresden, Germany*

[2] *London Mathematical Laboratory, 14 Buckingham Street, WC2N 6DF London, UK*

[3] *Centre de Recerca Matemàtica, Edifici C, Campus Bellaterra, E-08193 Barcelona, Spain.*

[4] *Departament de Matemàtiques, Facultat de Ciències, Universitat Autònoma de Barcelona, E-08193 Barcelona, Spain*

Abstract

We study the occurrence of events, subject to threshold, in a representative SOC sandpile model and in high-resolution rainfall data. The predictability in both systems is analyzed by means of a decision variable sensitive to event clustering, and the quality of the predictions is evaluated by the receiver operating characteristics (ROC) method. In the case of the SOC sandpile model, the scaling of quiet-time distributions with increasing threshold leads to increased predictability of extreme events. A scaling theory allows us to understand all the details of the prediction procedure and to extrapolate the shape of the ROC curves for the most extreme events. For rainfall data, the quiet-time distributions do not scale for high thresholds, which means that the corresponding ROC curves cannot be straightforwardly related to those for lower thresholds.

PACS numbers:

INTRODUCTION

Many atmospheric processes related to precipitation give rise to structures and correlations across long ranges in space and time, which are the result of the coupling between several non-linear mechanisms with different spatial and temporal characteristic scales [1–4]. Despite the diversity of individual rain events, an array of statistical measures presents strong statistical regularities [5–10], giving support to the hypothesis that atmospheric convection and precipitation may be a real-world example of self-organized criticality (SOC) [11]. Whereas the usual approach in meteorology and hydrology consists of looking at the occurrence of rain in fixed time intervals (days, months...), "episodic" rain events, similar to avalanches in SOC sandpile models, can be defined by integrating the rain rate over very short time periods. This led to the claim that rain-event sizes are power-law (i.e., scale-free) distributed, at least in the unique site studied [5], in agreement with the SOC hypothesis. Nevertheless, a power-law distribution of this observable is not sufficient evidence for SOC dynamics, as there are many alternative mechanisms that give rise to such behavior (see, for example, Refs. [12, 13]).

Further support for the SOC hypothesis was given by Peters and Neelin [6] who found, for rain data over the tropical oceans, (i) a relation between satellite estimates of rain rate and water vapor compatible with a phase transition, with large parts of the troposphere in a convectively active phase; and (ii) that the system was close to the transition point most of the time. This constitutes genuine evidence for SOC. These authors also related this SOC behavior to the concept of atmospheric quasi-equilibrium [14], which argues that, since driven processes are generally slow compared to convection, the system should typically be in a far-from equilibrium statistically stationary state, where driving and dissipation are in balance.

Coming back to local event-size distributions, recent works have shown that these are indicative of universality as expected in the SOC framework [8–10]. The resulting rain-event-size distributions for several sites distributed worldwide are well approximated by power laws of similar exponents over broad fitting ranges, with differences only in the large-scale cut-offs of the distributions. These differences are attributed to finite-size effects, pointing to distinct system capacities in different places.

This SOC framework raises the question of the possible implications of the critical be-

havior of atmospheric convection for the prediction of rainfall, which remain unclear, due to the fact that predictability in SOC systems is still not well understood. In particular, prediction studies often focus on the behavior of the most hazardous episodes, i.e. extreme events of rainfall in our case.

In a more general context, Kantz [15] classifies the different scientific approaches to extreme events, such as *extreme value statistics* for the robust estimation of the tails; *data driven predictions*, which employ conditional probabilities and temporal correlations; *simplistic physical models* to investigate the mechanisms and dynamics from which extreme events emerge; and *detailed disciplinary investigations* of extreme events in a particular system.

Our approach in this paper combines simplistic physical models (sandpile models) and data driven prediction in order to gain insight into rainfall occurrence, as well as a deeper understanding of SOC phenomena. Because a direct connection between sandpile-like models and rainfall has not yet been established, our purpose is not the modeling of the latter by the former, but rather the comparison of the dynamics of the two systems.

In the next section, we introduce the rain database and the SOC sandpile model used for comparison, and we define the extreme events of interest and present distributions of the quiet times that separate them. In Section III, we explain the prediction procedure, which makes use of the hazard function, and evaluate the predictability via the receiver operating characteristics (ROC) method. Section IV explores the prediction procedure analytically.

RAINFALL DATA AND SOC MODELS

We analyze high-resolution local rain intensities across different climates from the Atmospheric Radiation Measurement (ARM) database, and simulated data from the Manna sandpile model. The rain data consists of point-location measurements from sites around the world, with one minute temporal resolution spanning about 8 months to 7 years, depending on the site. For more details, see Ref. [8, 10]. The signal directly measured is the rain rate, giving the "instantaneous" depth of precipitation at a point location every minute, with a resolution of 0.001 mm/hour. In fact, anything below 0.2 mm/hour should be considered as zero, because it is not possible to distinguish rainfall from other phenomena such as mist. A rain "event" is defined as a sequence of rates exceeding a threshold r_c. To be precise,

the event starts when the threshold is exceeded for the first time and ends when the rate subsequently falls below threshold. Previous works on rainfall considered only the minimum possible threshold. However, this is not a fundamental physical parameter but rather an unavoidable limitation of the observational procedure. In this paper we are interested in exploring a range of thresholds, starting at the minimum reliable value of 0.2 mm/hour and working up to extreme thresholds.

As a prototypical SOC system we investigate the Abelian Manna sandpile model [16] in two dimensions. The model is defined on a two-dimensional square lattice of size L^2 with open boundaries. Each site $i = 1, \ldots, L^2$ contains a discrete number of particles z_i. The rules of the dynamics are:

1. Driving. A particle is added to a randomly chosen site i, $z_i \to z_i + 1$.

2. Toppling. If $z_i > 1$ at any site i, the site is relaxed, $z_i \to z_i - 2$, and the two particles are distributed among randomly and independently chosen nearest neighbours (nn), $z_{\rm nn} \to z_{\rm nn} + 1$ (with possibly the same site chosen twice). Multiple topplings are performed in parallel. This rule is iterated (if necessary) and each update defines one step in the "fast" avalanche time scale.

3. Dissipation. Particles that are distributed from edge sites beyond the boundaries of the lattice are removed from the system.

In the following, we drive the system 'infinitely slowly' (according to the usual protocol) by adding a new particle to the system only if all sites are relaxed. This effects a time-scale separation between driving and toppling. (For completeness, we also check the robustness of our results when this time-scale separation is broken, as in Refs. [17, 18].) Once the system has reached the statistically stationary state (i.e., the number of particles in the pile stabilizes, on average), the toppling activity n, which counts the number of toppling sites at each avalanche time step, is recorded. As with rain data, we make use of an activity threshold n_c and define events as consecutive sequences of $n > n_c$.

A key observable in our analysis (both for the rain data and the sandpile model) is the quiet time, τ, defined as the time the rate or activity signal spends below threshold. For the Bak-Tang-Wiesenfeld (BTW) model and other SOC models, it is well known that, if the system is slowly driven and the quiet time is measured in the slow time scale, the quiet-time

distribution is approximately exponential when $n_c = 0$, and therefore the instantaneous avalanches occur in the manner of a Poisson process [19], which, by definition, has no memory. Paczuski et al. [18] showed that this continues to hold even when the time-scale separation is broken (and one measures time on the avalanche time scale), provided $n_c = 0$.

At first sight, this observation appears to rule out the application of SOC models to real-world systems, such as solar flares or earthquakes, for which the quiet-time distributions are not exponential [20–22]. However, as shown in Ref. [18] for the BTW model, when a non-zero threshold is applied ($n_c > 0$), the quiet-time probability density function (PDF) is a decaying power law with exponent $\beta \approx 1.67$, independent of system size. This non-exponential PDF reflects the existence of clustering between events, in agreement with many natural phenomena. In the real world, thresholds are often imposed, e.g. because of the limited resolution of measuring devices, and therefore it is more realistic to consider non-zero thresholds for practical purposes.

Our simulations lead to very similar results for the Manna model with infinitely slow driving. Due to the time-scale separation, the quiet time is only defined inside the original, zero-threshold avalanches, and measured in the fast time scale, as in model A of Ref. [18]. Figure 1(a) shows, for a system of size $L = 1024$, quiet-time PDFs $P_q(\tau)$, where q denotes the thresholds as quantiles of the activity distribution. For any $n_c > 0$ (i.e., $q > 0$) the PDFs are clearly compatible with a power law with negative exponent $\beta = 1.67$ up until some fast-decaying cut-off. Although the cut-off function moves out with increasing threshold, a convincing data collapse onto a threshold-independent scaling function is possible, as shown in Fig. 1(b) (see also [8]). Similar behavior is observed when time-scale separation is broken by adding a particle to the system every 100 avalanche steps (whether or not all sites are relaxed). However, the scaling is not so clean: a bump appears between the power law and the subsequent faster decay (not shown). This arises from the mixture of quiet times within avalanches (corresponding to the previous case, model A) and exponential quiet times between avalanches.

Turning to rainfall data, Fig. 2 plots quiet-time PDFs $P_q(\tau)$ for different rate thresholds as measured at the ARM site on Manus island. Analyses for rate thresholds below 0.2 mm/h are disregarded owing to the detection limit on measurement devices. Thus, even for $q = 0$ an implicit threshold exists. Contrary to the Manna model, the PDFs are approximately independent of q up until about $q = 0.70$, following a power-law decay with an exponent

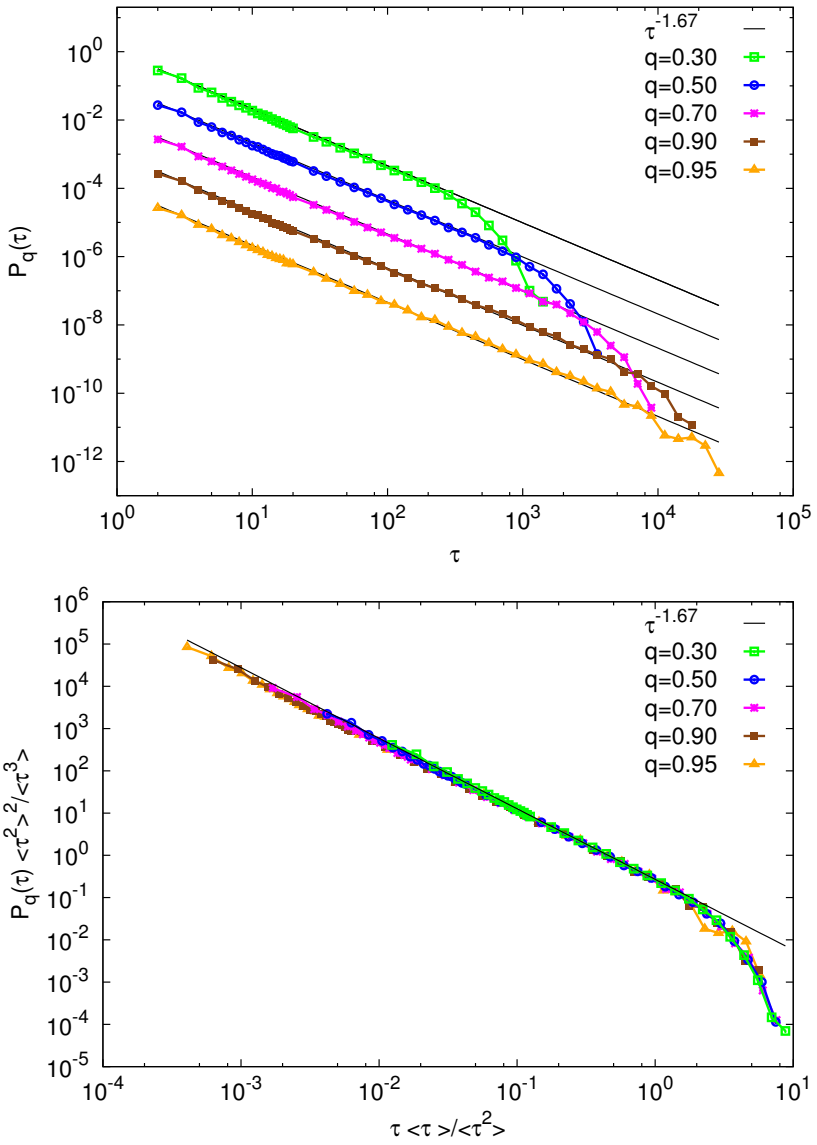

FIG. 1: (a) Quiet-time PDFs for the Manna model ($L = 1024$) for different activity thresholds n_c characterized by their quantiles q. Statistics are collected over 10^7 particle additions. PDFs for different q are displaced vertically for clarity. The solid black lines have slope -1.67. (b) Data collapse of the suitably rescaled quiet-time PDFs.

β close to 1.14 and a faster decay at the tail. Beyond $q = 0.70$, differences become more apparent. Nevertheless, a reasonable data collapse is shown in Fig. 2(b). Other ARM sites show roughly the same behavior. In the next two sections, we explore how differences in the quiet-time PDFs between the Manna model and rainfall data show up in the predictability of rain events.

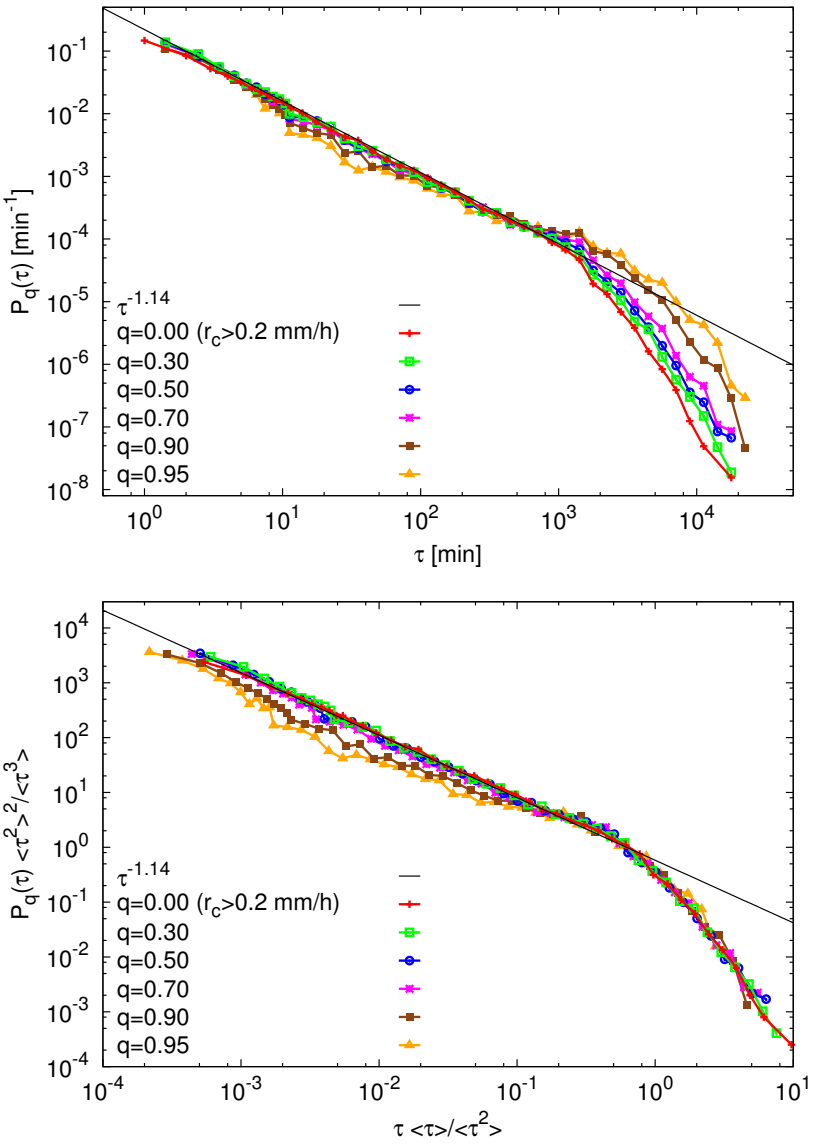

FIG. 2: (a) Quiet-time PDFs for different rain rate thresholds, as measured on Manus island for the period 2005/02/15 – 2012/03/18. A power law decay with exponent $\beta = 1.14$ has been fitted to the $q = 0.00$ data to serve as a visual guide. (b) Data collapse of the suitably rescaled quiet-time PDFs.

HAZARD FUNCTION AND ROC CURVES

For the purposes of time series prediction, we use the hazard function H_q (which is sensitive to both the clustering and repelling of events) as a decision variable. In comparison, the conventional precursory pattern recognition technique requires a large amount of data,

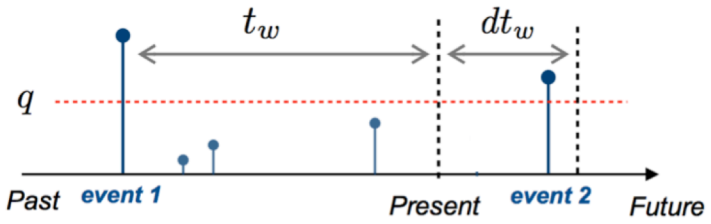

FIG. 3: Pictorial definition of the hazard function. Event 2 falls between t_w and dt_w, having exceeded event 1 by t_w.

does not capture long-term clustering, and has been found to perform worse in a similar analysis of heartbeat intervals [23]. The hazard function [24] gives the probability per unit time that the quiet time (for events defined by a threshold given by quantile q) terminates between t_w and $t_w + dt_w$, given that it has exceeded t_w, as illustrated in Fig. 3. That is,

$$H_q(t_w)dt_w = \frac{\int_{t_w}^{t_w+dt_w} P_q(\tau)\mathrm{d}\tau}{\int_{t_w}^{\infty} P_q(\tau)\mathrm{d}\tau} \tag{1}$$

$$= \frac{P_q(t_w)dt_w}{S_q(t_w)}, \tag{2}$$

where $S_q(t_w) = \int_{t_w}^{\infty} P_q(\tau)\mathrm{d}\tau$ is the survivor function [24], i.e., the probability that the quiet time is greater than t_w. For future reference it is useful to note that for exponential quiet times (Poisson process), the hazard function is constant. Since the time series under consideration are discrete, dt_w corresponds to one parallel update in the Manna model, and one minute for the rain data. The hazard function is constructed numerically via the quiet-time PDF and the survivor function. Figure 4 shows results for the Manna model and Manus island over the complete temporal record.

For the purposes of prediction we only assume access to past information, and the hazard function is therefore constructed solely from past events. We update its estimate every 100 events. Since the hazard function gives a probabilistic forecast, a deterministic prediction is issued via a discrimination threshold. Specifically, if in a given time step the estimated H_q exceeds the discrimination threshold, an alarm is raised, which is to say that an event is expected in the next dt_w. If H_q does not exceed the threshold, no alarm is raised and no event is expected.

We evaluate the quality of the prediction using a receiver operating characteristic (ROC) analysis [25]. For any binary prediction (alarm raised or not) there are four possible outcomes: an alarm is raised and the event does occur (true positive, TP); an alarm is raised

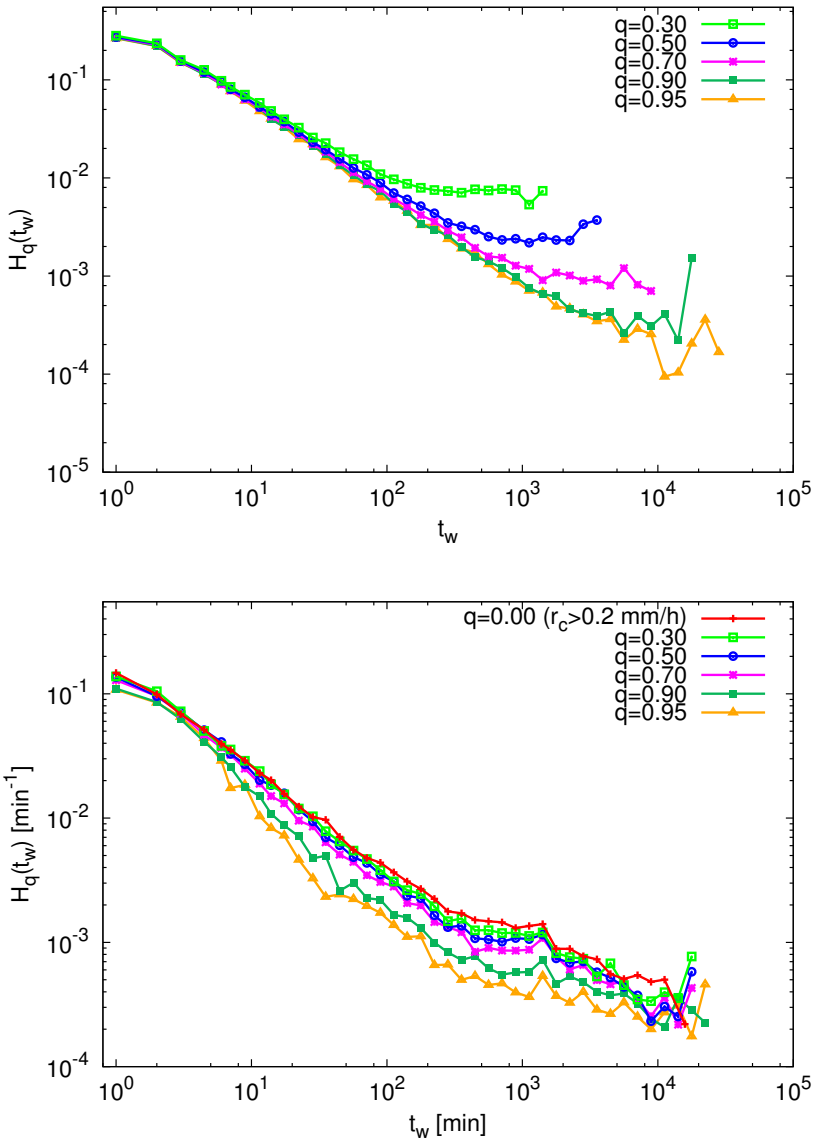

FIG. 4: (a) Hazard functions for quiet times in the Manna model for different activity thresholds (same data as in Fig. 1). (b) Hazard functions for quiet times of Manus island rain data for different rain rate thresholds (same data as in Fig. 2).

and the event does not occur (false positive, FP); an alarm is not raised and the event does occur (false negative, FN); an alarm is not raised and the event does not occur (true negative, TN). The ROC curve summarises this information by comparing the sensitivity (the proportion of successfully predicted occurrences) to the specificity (the proportion of successfully predicted non-occurrences):

$$\text{sensitivity} = \frac{\text{TP}}{\text{TP} + \text{FN}}, \qquad \text{specificity} = \frac{\text{TN}}{\text{TN} + \text{FP}}, \tag{3}$$

where TP, FN, TN, and FP refer to the number (or rate) of occurrences or non-occurrences for each case. Each threshold on the decision variable will give rise to a different point on the ROC curve. For example, in the absence of a threshold an alarm is raised every time step, such that FN = 0, yielding a sensitivity of 1. Such a protocol will never miss an occurrence, but will also never predict a non-occurrence, i.e., TN = 0, and therefore has specificity 0. On the other hand, for an unsurpassable threshold an alarm is never raised, such that FP = 0, yielding a specificity of 1. Such a protocol will never miss a non-occurrence, but will also never predict an occurrence and therefore has TP = 0 and sensitivity 0. The diagonal line in Fig. 5 that joins these two scenarios corresponds to non-informative predictions, i.e., issuing alarms at some fixed rate irrespective of the decision variable. Points above the diagonal represent good predictions and points below poor predictions, in comparison to totally random predictions. The point (1,1) corresponds to a perfect prediction.

Starting with the Manna model, the sequence of hazard functions in Fig. 4(a) suggests that the 'memory' between events persists for increasingly longer quiet times as the activity threshold is increased. This is inferred from the increasing crossover times to the constant 'memoryless' portion of the hazard curve. Thus, we anticipate that predictability improves with increasing activity threshold. This is indeed illustrated by the ROC curves in Fig. 5(a), which form an ordered sequence tending towards the corner (1,1) (perfect predictability). We will explore the clustering that gives rise to this increased predictability in the next section.

For rainfall data, the picture is more complicated. One can observe in Fig. 5(b) a bundle of ROC curves which are broadly similar up to thresholds of $q = 0.70$. For higher thresholds we find that, for sensitivities below 0.4, predictability (specificity) increases with threshold in rain rate (just as in the Manna model), but for higher sensitivities the opposite is true. Since low sensitivity corresponds to high thresholds in the hazard function (i.e. only events separated by short quiet times are successfully predicted), an increasing predictability implies that extreme events cluster more and more over short times. Conversely, high sensitivity corresponds to low thresholds in the hazard function (i.e. events separated by long quiet times are also successfully predicted), and a decreasing predictability implies that extreme events correlate less and less over long times. A closer re-examination of the highest quantile curves in Fig. 2(a) bears this out: the power-law exponent β appears to increase in the left part of the distribution, and the range of the exponential tail appears to increase in the right

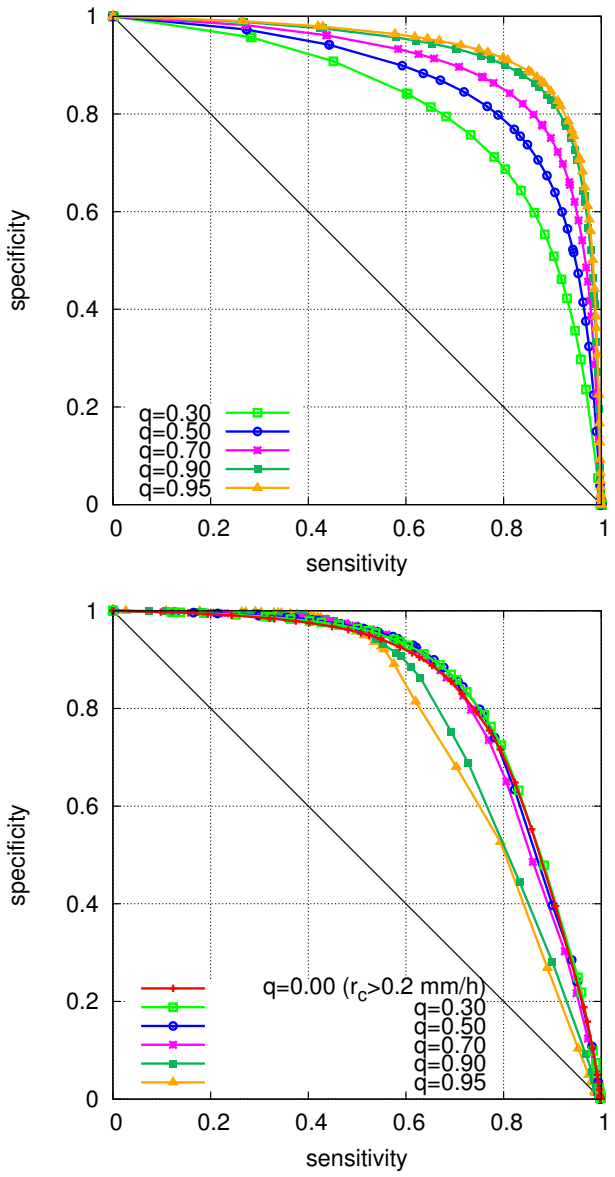

FIG. 5: ROC curves for different thresholds in the activity/rate for (a) the Manna model with $L = 1024$, (b) rainfall data from Manus island. Same data as in Figs. 1 and 2.

part. These longer times could be affected by seasonal effects which are difficult to resolve owing to the relatively short duration of the time series (7 years). Longer time series would be required in order to make better comparisons with SOC-like dynamics.

ANALYTICAL TREATMENT

For monotonically decaying hazard functions (as is approximately the case for the Manna model and rainfall, see Fig. 4), raising an alarm whenever the function exceeds a threshold

value is equivalent to raising an alarm all the while the elapsed time since the last event has not yet exceeded a 'threshold' time. This threshold time, Δ, is uniquely determined by the threshold imposed on the hazard function. Under these conditions it is possible to infer some general behaviour for the sensitivity and specificity. For simplicity, we will ignore any dependence on activity threshold in the following.

First, consider the sensitivity. Given an event, the subsequent event occurs either before the threshold time, $t_w \leq \Delta$, or after the threshold time $t_w > \Delta$. In the first case, events are successfully predicted, and therefore the total proportion of successfully predicted events $\mathrm{TP} \propto \int_0^\Delta P(\tau)d\tau = 1 - S(\Delta)$. The remaining proportion $S(\Delta) \propto \mathrm{FN}$ falls to unpredicted events, i.e., false negatives (recall the similarity with Type I errors in statistics). Thus,

$$\text{sensitivity } = 1 - S(\Delta),$$

which, if we introduce $\alpha = S(\Delta)$, is independent of the underlying form of the quiet-time distribution (apart from its assumed decaying monotonicity).

Next, consider the specificity. The specificity can also be calculated by instead considering non-events. Suppose an event takes place after a quiet time τ since the previous event. If $\tau < \Delta$ (with probability $1 - \alpha$), the contribution to false positives is proportional to τ, whereas the contribution to true negatives is zero (since the alarm will be raised all the while). If $\tau > \Delta$ (with probability α), the contribution to false positives is proportional to Δ, whereas the contribution to true negatives is proportional to $\tau - \Delta$ (since the alarm is no longer raised beyond Δ). Taking into account the condition $\tau \leq \Delta$ in the former case, the mean rate of false positives is thus

$$\mathrm{FP} \propto (1 - \alpha)\langle \tau | \tau \leq \Delta \rangle + \alpha\Delta.$$

Following the same reasoning, the rate of true negatives is

$$\mathrm{TN} \propto \alpha\langle (\tau - \Delta) | \tau > \Delta \rangle.$$

Therefore, as the proportionality factor is the same in both cases (associated with the elementary time step dt_w),

$$\text{specificity } = \frac{\alpha\langle (\tau - \Delta) | \tau > \Delta \rangle}{\alpha\langle (\tau - \Delta) | \tau > \Delta \rangle + (1 - \alpha)\langle \tau | \tau \leq \Delta \rangle + \alpha\Delta} = \frac{\alpha\langle (\tau - \Delta) | \tau > \Delta \rangle}{\langle \tau \rangle}, \qquad (4)$$

where $\langle \tau \rangle$ is the (unconditional) mean quiet time and $\langle (\tau - \Delta) | \tau > \Delta \rangle$ is the mean residual quiet time after an elapsed time Δ. This quantity has some counterintuitive properties in

the case of a decreasing hazard function [26, 27], but characterizes a random variable in the same way as its probability distribution (if the mean is finite [24]). In contrast to the sensitivity, the specificity does depend on the underlying form of the quiet-time distribution.

Eq. (4) provides the relation between specificity and sensitivity via Δ. For example, in the Poisson process the mean residual quiet time is equal to the mean quiet time irrespective of any elapsed time. Thus, specificity $= \alpha$ and so specificity $= 1-$ sensitivity.

It is instructive to apply the above analysis to a specific form of the quiet-time distribution. For the Manna model, this can be roughly modelled by a truncated gamma distribution

$$P(\tau) = \frac{1}{a\Gamma(\gamma, m/a)} \left(\frac{a}{\tau}\right)^{1-\gamma} e^{-\tau/a}, \tag{5}$$

where $m \geq 0$ is the lower cut-off of the distribution. The shape parameter $\gamma > 0$ for $m = 0$ and $-\infty < \gamma < \infty$ for $m > 0$, and the scale parameter $a > 0$ (which increases with activity threshold n_c, see Fig. 1(a)). The normalizing factor $\Gamma(\gamma, m/a)$ is the (upper) incomplete gamma function, defined by $\Gamma(\gamma, z) = \int_z^\infty x^{\gamma-1} e^{-x} dx$. Note that with this parameterization the power-law exponent is $\beta = 1 - \gamma$. Thus, comparing with the results of Sec. II for the Manna model, we have $\gamma = -0.67$. Also, exponential quiet times (as in a Poisson process) can be recovered as a special case by taking $\gamma = 1$, $m = 0$, and recalling that $\Gamma(1, z) = e^{-z}$.

From Eq. (5), the survivor function

$$S(\tau) = \int_\tau^\infty P(t_w) dt_w = \frac{\Gamma(\gamma, \tau/a)}{\Gamma(\gamma, m/a)}, \tag{6}$$

and the hazard function

$$H(\tau) = \frac{P(\tau)}{S(\tau)} = \frac{1}{a\Gamma(\gamma, \tau/a)} \left(\frac{a}{\tau}\right)^{1-\gamma} e^{-\tau/a}. \tag{7}$$

To compute the specificity, we require the mean quiet and mean residual quiet times, which are given by

$$\langle \tau \rangle = a \frac{\Gamma(\gamma + 1, m/a)}{\Gamma(\gamma, m/a)} \tag{8}$$

and

$$\langle \tau - \Delta | \tau > \Delta \rangle = \int_m^\infty (\tau - \Delta) P(\tau | \tau > \Delta) d\tau = \int_\Delta^\infty (\tau - \Delta) \frac{P(\tau)}{S(\Delta)} d\tau \tag{9}$$

$$= \frac{a}{\Gamma(\gamma, \Delta/a)} \int_\Delta^\infty \left(\frac{\tau}{a}\right)^\gamma e^{-\tau/a} \frac{d\tau}{a} - \Delta = a \frac{\Gamma(\gamma + 1, \Delta/a)}{\Gamma(\gamma, \Delta/a)} - \Delta, \tag{10}$$

for $\Delta > m$. This equation can be recast in a form more suggestive of scaling with the help of the identity $\Gamma(\gamma+1,z) = z^\gamma e^{-z} + \gamma\Gamma(\gamma,z)$, giving

$$\langle \tau - \Delta | \tau > \Delta \rangle = a\left[\left(\frac{\Delta}{a}\right)^\gamma \frac{e^{-\Delta/a}}{\Gamma(\gamma,\Delta/a)} + \gamma - \frac{\Delta}{a}\right]. \tag{11}$$

As noted previously, high activity thresholds correspond to large values of the scale parameter a, while the lower cut-off m is essentially fixed by the available time resolution, e.g. one time step in the Manna model. Therefore, in order to explore scaling behaviour of the sensitivity and specificity, we consider the limit $m/a \to 0$ (with m constant), in which case

$$\frac{1}{\Gamma(\gamma,m/a)} \simeq \begin{cases} 1/\Gamma(\gamma) & \gamma > 0 \\ -\gamma(m/a)^{-\gamma} & \gamma < 0, \end{cases} \tag{12}$$

with $\Gamma(\gamma) = \Gamma(\gamma,0)$ if $\gamma > 0$, see Ref. [28]. Proceeding to the quantities that appear in the ROC curves, we have

$$S(\Delta) \simeq \begin{cases} f_+(\Delta/a) & \gamma > 0 \\ a^\gamma f_-(\Delta/a) & \gamma < 0, \end{cases} \tag{13}$$

$$\langle \tau - \Delta | \tau > \Delta \rangle \simeq a f_2(\Delta/a) \quad \text{for all } \gamma \tag{14}$$

$$\langle \tau \rangle \simeq \begin{cases} a\gamma & \gamma > 0 \\ -a^{1+\gamma} m^{-\gamma}\gamma\Gamma(\gamma+1) & -1 < \gamma < 0 \\ m\gamma/(\gamma+1) & \gamma < -1, \end{cases} \tag{15}$$

where f_+, f_-, and f_2 are different scaling functions. Collecting these results, we have

$$\text{specificity} = \begin{cases} f_3(\Delta/a) & \gamma > -1 \\ a^{\gamma+1} f_3(\Delta/a) & \gamma < -1, \end{cases} \tag{16}$$

where f_3 is another scaling function. The sensitivity $= 1 - S(\Delta)$, meanwhile, scales differently for $\gamma > 0$ and $\gamma < 0$. Thus, we finally obtain

$$1 - \text{sensitivity} = \begin{cases} f_4(\text{specificity}) & \gamma > 0 \\ a^\gamma f_4(\text{specificity}) & -1 < \gamma < 0 \\ a^\gamma f_4(\text{specificity}/a^{\gamma+1}) & \gamma < -1, \end{cases} \tag{17}$$

where f_4 is another scaling function. An important consequence of these results is that for $\gamma > 0$ predictability is independent of a, whereas for $-1 < \gamma < 0$ sensitivity increases with

a for a fixed specificity. In this sense, extreme events are more predictable, as in Ref. [19], but for different reasons. In fact, the sensitivity tends to one as $a \to \infty$ for any non-zero specificity. This is in agreement with our findings for the Manna model.

A concrete validation of this analysis can be achieved by plotting,

$$\text{specificity versus } \frac{1-\text{sensitivity}}{\langle\tau^2\rangle^\gamma/\langle\tau\rangle^\gamma},$$

which makes use of the fact that the scale parameter a is proportional to $\langle\tau^2\rangle/\langle\tau\rangle$ when $-1 < \gamma < 0$, see Refs. [8, 29]. Noting that $a^\gamma \propto \langle\tau\rangle^2/\langle\tau^2\rangle$, a non-parametric version of the scaling law for the ROC curve reads

$$\text{specificity versus } \frac{1-\text{sensitivity}}{\langle\tau\rangle^2/\langle\tau^2\rangle},$$

which is also valid for when $-1 < \gamma < 0$ [29], and displayed in Fig. 6 for the Manna model. The scaling is reasonable but not perfect. For a better approximation the finiteness of the time resolution, i.e., the fact that $m < 0$ should be take into account in the calculation of the specificity, Eq. (4). If m is not negligible, then the FP rate is reduced by a term proportional to m, which leads to the replacement of $\langle\tau\rangle$ by $\langle\tau\rangle - m$ in the denominator of Eq. 4. This means that all the previous equations remain valid if the specificity is multiplied by a factor $1 - m/\langle\tau\rangle$. Thus, the scaling of the ROC curve is generalized to

$$\text{specificity} \times \left(1 - \frac{m}{\langle\tau\rangle}\right) \text{ versus } \frac{1-\text{sensitivity}}{\langle\tau\rangle^2/\langle\tau^2\rangle}.$$

Although this scaling theory works well for the Manna model, the collapse of the ROC curves for rainfall is poor (not shown), because the quiet-time distributions do not scale for high rain-rate thresholds.

As a final comment, although we have carried out this analysis for a truncated gamma distribution, we expect the previous scaling results to hold for any quiet-time distribution of the form

$$P(\tau) = \frac{1}{\tau^{1-\gamma}} f_0(\tau/a),$$

where f_0 is a scaling function taking a constant value for small arguments and decaying fast enough for large arguments. The normalization constant hidden in f_0 may also depend on a.

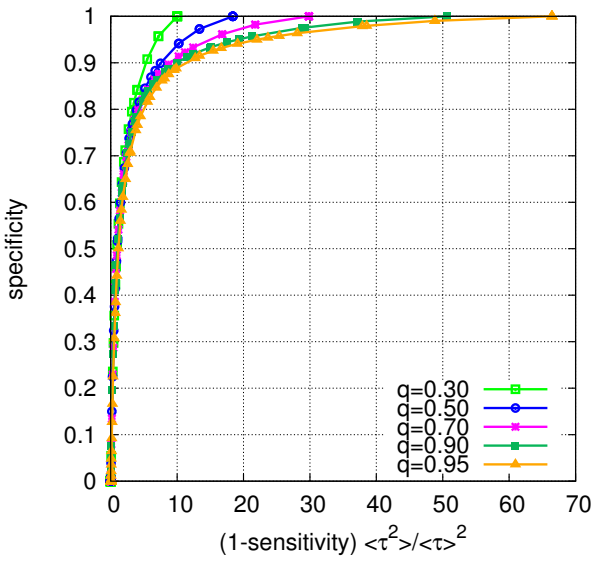

FIG. 6: Data collapse after rescaling the ROC curves for different activity thresholds in the Manna model with $L = 1024$. Same data as in Fig. 1.

CONCLUSIONS

In summary, we have studied the effect of thresholding in a representative SOC model and on actual rainfall data. The predictability of events is studied by means of a decision variable sensitive to the tendency of the events to cluster or repulse, and the quality of the predictions is evaluated by the ROC method. Thresholds have been applied to the rate or activity, which, in the context of SOC models, corresponds to observing the process on the fast (avalanche) time scale. In this case, the relative weight of the exponential tail decreases as the threshold increases, leading to higher predictability. For rainfall data, however, the change in the ROC curves with threshold is less clear, since the quiet-time distributions do not seem to scale for high thresholds. A scaling theory developed for the Manna model, valid for any system in which the quiet-time distribution scales with threshold, helps us understand all the details of the prediction procedure. The philosophy of our paper is similar to that of Ref. [30], but note that in that work the prediction scheme is based on precursory structures rather than the hazard function.

Clearly, our prediction method works best for renewal processes (point processes in which the quiet times are independent of each other). Analogies with other natural hazards [31] suggest that the renewal process is just a first approximation. Extensions to our approach

would therefore include previous history, such that the hazard function is a function of previous quiet times. Nevertheless, our analytical approach is valid for any point process to which our prediction procedure is applied (not only for renewal processes). Further refinements would include knowledge of the rain rate or toppling activity below threshold. These extensions are left for future research.

ACKNOWLEDGEMENTS

Rain data was obtained from the Atmospheric Radiation Measurement Program sponsored by the US Department of Energy, Office of Science, Office of Biological and Environmental Research, Environmental Sciences Division. The authors were introduced in rain research by Ole Peters. Research expenses were founded by projects FIS2009-09508, from the disappeared Spanish MICINN, FIS2012-31324, from Spanish MINECO, and 2009SGR-164 and 2014SGR-1307, from AGAUR. A.D. is grateful for the hospitality of the Max Planck Institute for the Physics of Complex Systems and the Universidade Federal de Minas Gerais.

---

* Electronic address: adelucasilberberg@gmail.com

† Electronic address: acorral@crm.es

[1] S. Lovejoy. Area-perimeter relation for rain and cloud areas. *Science*, 216:185–187, 1982.

[2] G. Vattay and A. Harnos. Scaling behavior in daily air humidity fluctuations. *Phys. Rev. Lett.*, 73:768–771, 1994.

[3] J. I. Yano, R. Blender, C. Zhang, and K. Fraedrich. 1/f noise and pulse-like events in the tropical atmospheric surface variabilities. *Q. J. R. Meteorol. Soc.*, 130:1697–1721, 2003.

[4] E. Bodenschatz, S. P. Malinowski, R. A. Shaw, and F. Stratmann. Can we understand clouds without turbulence? *Science*, 327(5968):970–971, 2010.

[5] O. Peters, C. Hertlein, and K. Christensen. A complexity view of rainfall. *Phys. Rev. Lett.*, 88:018701, 2002.

[6] O. Peters and J. D. Neelin. Critical phenomena in atmospheric precipitation. *Nature Phys.*, 2:393–396, 2006.

[7] J. D. Neelin, O. Peters, J. W.-B. Lin, K. Hales, and C. E. Holloway. Rethinking convec-

tive quasi-equilibrium: observational constraints for stochastic convective schemes in climate models. *Phil. Trans. R. Soc. A*, 366:2581–2604, 2008.

[8] O. Peters, A. Deluca, A. Corral, J. D. Neelin, and C. E. Holloway. Universality of rain event size distributions. *J. Stat. Mech.*, P11030, 2010.

[9] A. Deluca and A. Corral. Scale invariant events and dry spells for medium-resolution local rain data. *Nonlinear Proc. Geophys.*, 21:555–567, 2014.

[10] A. Deluca, P. Puig, and A. Corral. Testing universality in critical exponents: the case of rainfall. *In progress*, 2014.

[11] P. Bak, C. Tang, and K. Wiesenfeld. Self-organized criticality: an explanation of $1/f$ noise. *Phys. Rev. Lett.*, 59:381–384, 1987.

[12] R. Dickman. Rain, power laws, and advection. *Phys. Rev. Lett.*, 90(10):108701(1–4), 2003.

[13] M. Mitzenmacher. A brief history of generative models for power law and lognormal distributions. *Internet Math.*, 1 (2):226–251, 2004.

[14] A. Arakawa and W. H. Schubert. Interaction of a cumulus cloud ensemble with the large-scale environment, part I. *J. Atmos. Sci.*, 31:674–701, 1974.

[15] H. Kantz. Dynamics and statistics of extreme events. In E. Estrada, M. Fox, D. J. Highman, and G. O, editors, *Network Science*, pages 205–216. Springer, 2010.

[16] D. Dhar. The abelian sandpile and related models. *Physica A*, 263(1):4–25, 1999.

[17] A. Corral and M. Paczuski. Avalanche merging and continuous flow in a sandpile model. *Phys. Rev. Lett.*, 83:575–578, 1999.

[18] M. Paczuski, S. Boettcher, and M. Baiesi. Interoccurrence times in the Bak-Tang-Wiesenfeld sandpile model: A comparison with the observed statistics of solar flares. *Phys. Rev. Lett.*, 95:181102, 2005.

[19] A. Garber, S. Hallerberg, and H. Kantz. Predicting extreme avalanches in self-organized critical sandpiles. *Phys. Rev. E*, 80:026124, 2009.

[20] G. Boffetta, V. Carbone, P. Giuliani, P. Veltri, and A. Vulpiani. Power laws in solar flares: Self-organized criticality or turbulence? *Phys. Rev. Lett.*, 83:4662–4665, 1999.

[21] A. Corral. Long-term clustering, scaling, and universality in the temporal occurrence of earthquakes. *Phys. Rev. Lett.*, 92:108501, 2004.

[22] A. Corral. Comment on "Do earthquakes exhibit self-organized criticality?". *Phys. Rev. Lett.*, 95:159801, 2005.

[23] M. I. Bogachev, I. S. Kirrenkov, E. M. Nifotov, and A. Bunde. Statistics of return intervals between long heartbeat intervals and their usability for online prediction of disorders. *New J. Phys.*, 11(063036):1–19, 2009.

[24] J. D. Kalbfleisch and R. L. Prentice. *The Statistical Analysis of Failure Time Data*. Wiley, Hoboken, NJ, 2nd edition, 2002.

[25] J. P. Egan. *Signal Detection Theory and ROC Analysis*. Academic Press, New York, 1975.

[26] P. M. Davis, D. D. Jackson, and Y. Y. Kagan. The longer it has been since the last earthquake, the longer the expected time till the next? *Bull. Seismol. Soc. Am.*, 79:1439–1456, 1989.

[27] A. Corral. Time-decreasing hazard and increasing time until the next earthquake. *Phys. Rev. E*, 71:017101, 2005.

[28] M. Abramowitz and I. A. Stegun, editors. *Handbook of Mathematical Functions*. Dover, New York, 1965.

[29] A. Corral. Scaling in the timing of extreme events. *arxiv.org*, 1408.1943, 2014.

[30] S. Hallerberg and H. Kantz. Influence of the event magnitude on the predictability of an extreme event. *Phys. Rev. E*, 77:011108, 2008.

[31] A. Corral. Dependence of earthquake recurrence times and independence of magnitudes on seismicity history. *Tectonophys.*, 424:177–193, 2006.